Efficient Electrochemical Reduction of CO_2 to Formate in Methanol Solutions by Mn Functionalized Electrodes in the Presence of Amines

Francesca Marocco Stuardi,[a] Arianna Tiozzo,[b] Laura Rotundo,[b,c] Roberto Gobetto,*[b] Carlo Nervi,*[b] Julien Leclaire*[a]

Carbon cloth electrode modified by covalently attaching a manganese organometallic catalyst is used as cathode for the electrochemical recuction of CO_2 in methanol solutions. Six different amines are employed as co-catalyst in millimolar concentrations, which coupled to the increased solubility of CO_2 in methanol enhance the formate production, switch the selectivity toward formate anion, and in the case of pentamethyldiethylentriamine (PMDETA) resulted in an impressive TON_{HCOO^-} of 2.8×10^4. We demonstrate that the protonated PMDETA is formed in methanol solution by simply bubbling CO_2, which is the responsible for a barrierless transformation of CO_2 to formate via the reduced form of the Mn catalyst covalently bonded to the electrode surface. These findings pave the way for more efficient transformation of CO_2 into liquid fuel and shed light on the electrochemical mechanism

.

Introduction

The development of efficient catalysts for the electrochemical reduction of CO_2, a very active research topic, should not be envisaged in the sole framework of CO_2 utilization, but rather as a brick of an entire carbon capture, utilization and storage (CCUS) value chain. Recent reports pointed out that an integrated approach, wherein the capture, utilization and storage technologies are designed to operate synergistically, may represent one of most effective options for viable and scalable GHG (Green House Gases) mitigation.[1,2]

Post-combustion CO_2 capture is the most mature technology for flue gas treatment, and it is already implemented into existing power plants. To process diluted and low-pressure streams, such as those emitted by fossil-fired power plants, chemical absorption with aqueous amine solutions, called amine-scrubbing, is the most appropriate technology.[3-6] Amines spontaneously react with CO_2 affording equilibrated mixtures of ammonium carbamates (Scheme 1, eq. 1) and bicarbonate (in the presence of water, Scheme 1, eq. 2). Captured CO_2 can be released by thermally reversing these reactions, but the associated energetic cost is one of the major drawbacks.[7]

In situ direct transformation of captured CO_2 (in the form of ammonium carbamate or bicarbonate) is a challenging alternative, which fits into the aforementioned process integration paradigm. Although most CO_2 utilization processes reported to date operate from purified CO_2, there has been a growing interest for the direct conversion of capture products in the past decade.[8] These examples include the utilization of carbamates as metal extractants[6], as vehicles for mineral carbonation[9], or their conversion into renewable fuels such as methanol.[8, 10]

The latter is a true transformation, not a utilization but it raises the issue of the electron source needed to produce hydrogen, itself required for CO_2 reduction. Using renewable electrical energy (i.e. photochemical or electrochemical reductions[11-14]) for CO_2 reduction surely represents a step further toward true sustainable CCUS but also an additional challenge. Yet, photochemical or electrochemical reduction strategies enabling to produce C1 and C2 chemicals from flue gases will certainly be one of the essential bricks of the next industrial revolution.[15, 16]

The main products of CO_2 electrolysis are usually CO, CH_4, C_2H_4, formate, CH_3OH and CH_3CH_2OH,[17] which are valuable feedstocks for the chemical industry and for energy storage. A large array of transition metal complexes[18] containing macrocyclic, (e.g. porphyrins, phthalocyanines, corroles and cyclams),[19-21] polydentate, (e.g. 2,2'-bipyridine (bpy), 1,10-phenantroline (phen), etc.)[22-24] and phosphine ligands (e.g. 1,2-bis(diphenylphosphino)ethane (dppe), triphenylphosphine (PPh_3), etc.)[25-27] have been tested as molecular electrocatalysts in solutions, wherein CO_2 was injected as a pure gas. Re- and Mn-polypyridine complexes were shown to be among the most promising catalysts, displaying high reaction rates and selectivity. As a consequence, their reduction mechanisms were extensively explored. By fine-tuning electronic properties and steric hindrance around the metal centre, the selectivity and the activity of the electrocatalyst can be controlled.[28-30] The availability of local proton sources is known to greatly impact these two parameters, potentially enabling to shift the CO_2 reduction process from the production of CO to formate.[29, 31] In particular, polypyridyl Mn(I) catalysts (e.g. [Mn(pdbpy)$(CO)_3$Br] (pdbpy = 4-phenyl-6-(phenyl-2,6-diol)-2,2'-bipyridine) containing two acidic OH groups in proximity of the purported metal binding site for CO_2 redox catalysis show enhanced catalytic activity towards HCOOH production.[32, 33]

As mentioned earlier, examples of electrochemical CO_2 reduction integrated to its absorption remain scarce.[34-36] To our knowledge, only two studies to date reported the reduction of CO_2 with a Mn-based soluble electrocatalyst, in the presence of amines (in solution or bound to the metal chelating unit).[34] Amine moieties were proposed not only to provide binding sites, hence a reservoir of CO_2 under the form of carbamates, but also to stabilize and promote the formation of the hydride catalytic intermediate (**HMn**), thereby favouring formate production instead of CO.[36, 37] These amines, which are supposed to work as proton shuttle, were either introduced in large excess with respect the catalyst[34] or upon an elaborated

synthetic procedure as a side-arm of the Mn catalyst (Figure 1).[37] Hydride transfer to CO_2 requires a proton source, a role which was endorsed by acidic alcohols such as phenols or perfluoroalcohols. None of this class of sacrificial proton donors seems eligible for potential implementation into a cost-effective industrial process, while water suffers from low CO_2 solubility.
To enable the industrial utilization of CO_2 for energy production,

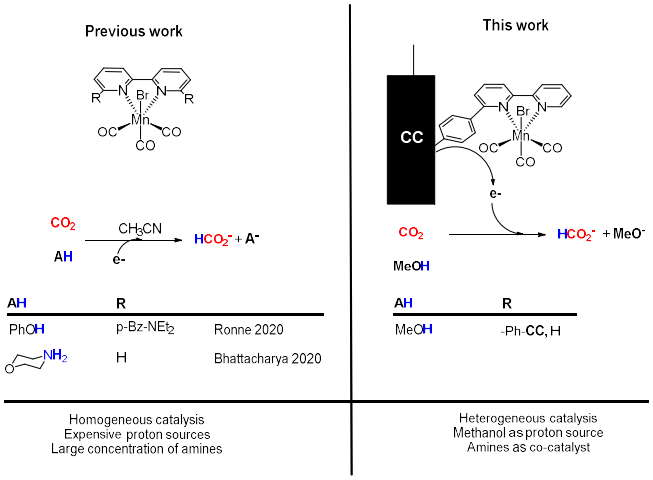

Figure 1: Schematic representation of the differences between previous integrated CO_2 reduction systems in the presence of amines with homogeneous Mn bipyridyl complexes and the current work.

liquid fuels (i.e. formate) rather than gas precursors (i.e. CO) should be preferred for safety, storage and transportation reasons. In the same perspective of deployment, the immobilization of organometallic complexes onto a conductive support (*via* van der Waals interactions[38, 39] or by the formation of a covalent bond between the electrode surface and the intact transition metal catalysts[40, 41]) is highly desirable. It enables to envisage a broader scope of solvents, including carbon capture media, and provides the reduction systems with increased durability, efficiency, recyclability and processability.[40, 41]
Herein we investigate the role and impact of amines in millimolar concentration on the electroreduction of CO_2 by a Mn bipyridyl complex (*fac*-Mn(apbpy)$(CO)_3$Br [apbpy=4-(4-aminophenyl)-2,2'-bipyridine)]) covalently bound to a Carbon Cloth (**CC**) surface. **CC** is a relatively cheap material of low electrical resistance and large surface area, widely exploited for the preparation of electrodes for low temperature fuel cells.[42] The functionalized electrode (**Mn/CC**) was tested as a catalyst for CO_2 electrochemical reduction in a three-electrode cell with two gastight compartments, with methanol as a solvent. Its performance was studied in the presence of a panel of industrial amines (Figure 2) by means of Controlled Potential Electrolysis (CPE).
By a combination of theoretical and experimental investigations, we herein show that methanol acts at the same time as a carbon solvent, enhancing CO_2 solubility compared to water, and as an affordable sacrificial proton source. In our system, amines rather play the role of homogeneous co-catalysts or co-factors during the reduction process. Combining a heterogeneous catalysis approach and a more accessible sacrificial proton source may also pave the way toward scalable capture and integrated electroreduction processes.

C_0 (mM)									K(H_2O)[a]	K(MeOH)[b]
1		50		175						
2 R_2NH	+			CO_2	(1) ↔	$R_2NH_2^+$	+	$R_2NCO_2^-$	1.2×10^4	1.9×10^1
R_3N	+	H_2O	+	CO_2	(2) ↔	R_3NH^+	+	HCO_3^-	5.5×10^2	1.1×10^1
$R_2NCO_2^-$	+	H_2O			(3) ↔	R_2NH	+	HCO_3^-		
1-x						x		x		

Scheme 1. CO_2 capture equilibria at work in our system, maximal concentration of species and related binding constants. (1) carbamation; (2) carbonation; (3) carbamate hydrolysis. a from ref[43]; b : from ref[6], see supporting section S6

Results and discussion

fac-Mn(apbpy)$(CO)_3$Br was anchored to a carbon cloth (**CC**) electrode surface via the formation of C–C bonds. The presence of the aniline moiety on the bipyridyl ligand enables the grafting of the complex onto carbon surfaces via the *in situ* formation of the corresponding diazonium salt (see supporting section 4). This method advantageously bypasses the isolation and purification of the diazonium reactive intermediate. Electrochemical reduction is performed to trigger C–C bond formation and N_2 evolution. To assess the amount of electrocatalyst covalently bound on **CC**, a comparative ICP analysis was performed on the pristine **CC** starting material and on **Mn/CC** (see supporting section 4). A surface coverage Γ of 1.67×10^{-9} mol cm_{ECSA}^{-2} was obtained, in reasonable agreement with the previously reported value (1.4×10^{-9} mol cm_{ECSA}^{-2}), determined via the indirect method of charge integration of the CV data collected from **CC** bonded nitroaniline.[40, 41]

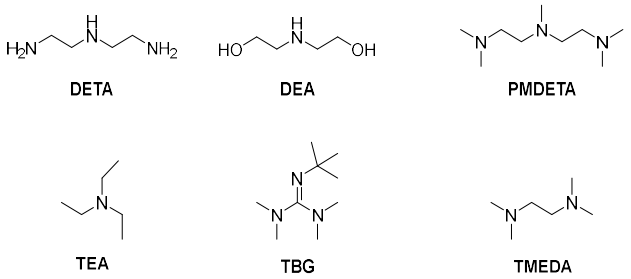

Figure 2: Panel of industrial amines (and guanidine) tested in this work.

state	ΔG° (kJ·mol^{-1})	Conc (mM)
atm		0.018
Flue		5.4
Pure gas	+9.0	45
Dissolved[a]	–12.9	175
bicarbonate[b]	–28.6	< 3
carbamate[b]	–36.4	< 1.5

Table 1: Gibb's free enthalpies of CO_2 in different states and concentrations used in the present study. [a] Calculated from CO_2 solubility in MeOH. [b] From MEA in water (from ref [43]).

The modified **CC** electrode was first tested for CO_2 electroreduction using a three-electrode cell with two gastight compartments filled with methanol, kept under a constant flow of CO_2 (30 mL/min). An onset reduction potential of –1.35 V vs Ag/AgCl was applied.

With the exact same setup, CO_2 reduction was performed with the **Mn/CC** modified electrode immersed into CO_2-saturated MeOH solution of each amine (1 mM) within the cathodic compartment. The different amines tested (Figure 2) were Diethylenetriamine (**DETA**), Diethanolamine (**DEA**), Pentamethyldiethylentriamine (**PMDETA**), Triethylamine (**TEA**), Tetramethyletylendiamine (**TMEDA**) and 2-tert-butyltetramethylguanidine (**TBG**).

At such a low amine concentration (1 mM), at least three orders of magnitude lower than what is commonly used for CO_2 capture (MEA 5 M, 30% w/w), most of the captured CO_2 is absorbed by physical dissolution (see Table 1). In fact, at room temperature and under a partial pressure p(CO_2) = 1 atm, this gas has a solubility of 0.007 in MeOH,[44] which translates into a concentration around 175 mM. Although our amine solutions are rather diluted (1 mM), the values of carbamation and carbonation equilibrium constants (Scheme 1) suggest that these processes remain quantitative in our operational conditions (see supporting section 5 for the relationship between binding constant per nitrogen site and per absorbent molecule). This was experimentally verified by ^{1}H NMR for **DEA**, **DETA** and **PMDETA**, which cover the scope of primary to tertiary amines, bearing between one and three binding sites and either undergoing preferentially carbamation or carbonation (see SI section 7). As Gibb's free energy of carbonation is lower compared to carbamation, we herein used a 50-fold excess of water with respect to the amine, which enables the former process to be as favoured as the latter (Table 1 and Scheme 1, eq. 2). In our operating conditions, amines are stoichiometrically loaded with CO_2. Yet, these adducts cannot be realistically considered as substrates for CO_2 conversion, as they are 100 times less abundant than dissolved CO_2. In addition, and as reported in Table 1, they are also substantially more stabilized than the dissolved gas. In such conditions, the scenario wherein ammonium carbamates and carbonates (more stable and less abundant than dissolved CO_2) act as substrates during electroreduction can eventually be ruled out, allowing us to focus on the potential role of these CO_2-amine derivatives in the very catalytic process. We have recently shown that industrial polyamines used for CO_2 capture are powerful metal chelators which can effectively be employed for metal extraction in methanolic medium. In agreement with this previous study, we observed that 20 minutes of CO_2 flow were required to fully pre-load the amine solution and further enable the electrolysis to proceed properly. Any attempt to directly contact the unloaded diluted amine and the catalyst, systematically resulted in a detrimental effect on the reduction activity. In addition, DFT calculations also suggests that the real catalyst (i.e. the Mn pentacoordinate anion $[Mn(bpy)(CO)_3]^-$, **Mn$^-$**, see Scheme 2 below) prefers to coordinate the free amine rather than CO_2 or MeOH (see supporting section 8). After the preliminary CO_2 saturation, **Mn/CC** was inserted in solution, continuously supplied with CO_2 while the electrolysis was

diluent	Amine (1 mM)	Time (h)	TON_{CO}	TON_{H2}	TON_{HCOO-}	FE_{CO} (%)	FE_{H2} (%)	FE_{HCOO-} (%)
Water	-[a]	10	33200	28800	0	60	40	0
methanol	–	22	10360	3900	5150	51	20	26
	DETA	22	7960	3860	16160	26	12	51
	DEA	20	8530	6230	7780	29	21	25
	PMDETA	22	3000	6700	28000	5	11	66
	TEA	21	5735	6740	4040	20	23	15
	TBG	22	6159	5613	6563	21	19	22
	TMEDA	15	10073	16771	873	26	44	3

Table 2. TONs and FE values for CO_2 reduction with the **Mn/CC** electrode in MeOH ($TBAPF_6$ 0.1 M as supporting electrolyte) with and without amines (1 mM). [a] water solutions with no added amines (Ref. [40]).

conducted with a set potential of –1.35 V vs. Ag/AgCl. Karl-Fischer titrations were performed at the beginning and at the end of the process, confirming that a constant amount of H_2O was present in the medium, around 0.96 mg/mL (i.e. 0.1 % w/w or 50 mM).

Table 2 shows the TONs (Turnover Numbers) and FEs (Faradic Efficiencies) obtained for all the different conditions tested. TON_{CO}, TON_{H2} and corresponding FE values were obtained by sampling gases from the cell headspace every 5 minutes and by injecting them in a micro-GC analyzer, while TON_{HCOO-} and FE_{HCOO-} were evaluated by quantitative ^1H NMR analysis of the catholyte at the end of electrolysis.

Figure 3 displays the overall TON_{H2}, TON_{CO} and TON_{HCOO-} values after 22 hours of continuous CPE at –1.35 V for all amines (E_{red}=–1.35 V, $TBAPF_6$ 0.1 M), and the production of H_2 and CO over time of a methanolic solution containing **PMDETA**.

Some general observation can be made from the results gathered in Figure 3 and Table 2. We previously reported that the same **Mn/CC** catalyst only afforded CO (FE_{CO} = 60%) and H_2 (FE_{H2} = 40%) as CO_2 reduction products when used in aqueous medium,[40] while CPE in MeOH displays FE_{CO} = 51%, Fe_{H2} = 20% and FE_{HCOO-} = 26% (Table 2). It is now accepted that the production of formate occurs via the formation of the hydride **HMn** intermediate, while CO_2 reaction with the active catalysts

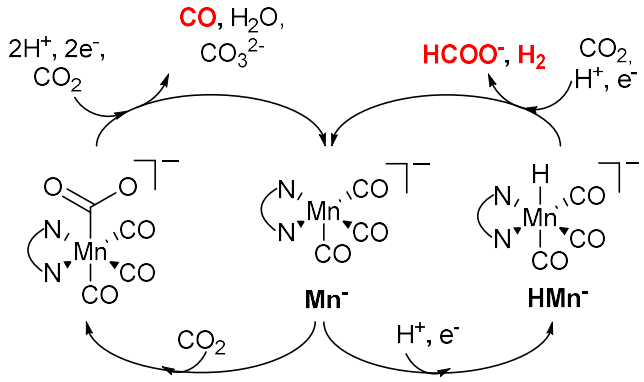

Scheme 2. Schematic mechanism of CO_2 reduction by Mn catalysts.

Mn$^-$, followed by the protonation-first or reduction-first mechanisms lead to CO (Scheme 2).[33, 37, 45]

Clearly, by simply switching from aqueous to methanolic solutions, a change in reduction selectivity occurs. The same shift in selectivity in favour of formate (path via **HMn**$^-$ in Scheme 2) may be obtained in water by using gas diffusion layer (GDL) electrochemical cell, resulting into FE_{CO} = 76.2%, FE_{H2} = 13.7% and FE_{HCOO-} = 10.1%.[41] The effect has been ascribed to acidification induced by increased CO_2 concentrations, symptomatic of GDL cells. Following this track, we tried to further shed light on the chemical process leading to formate production in methanol. This may either be imputed to higher CO_2 concentration (as in water[40, 41]) and, when any, to a non-innocent-role played by the amine in the catalytic reduction mechanism.

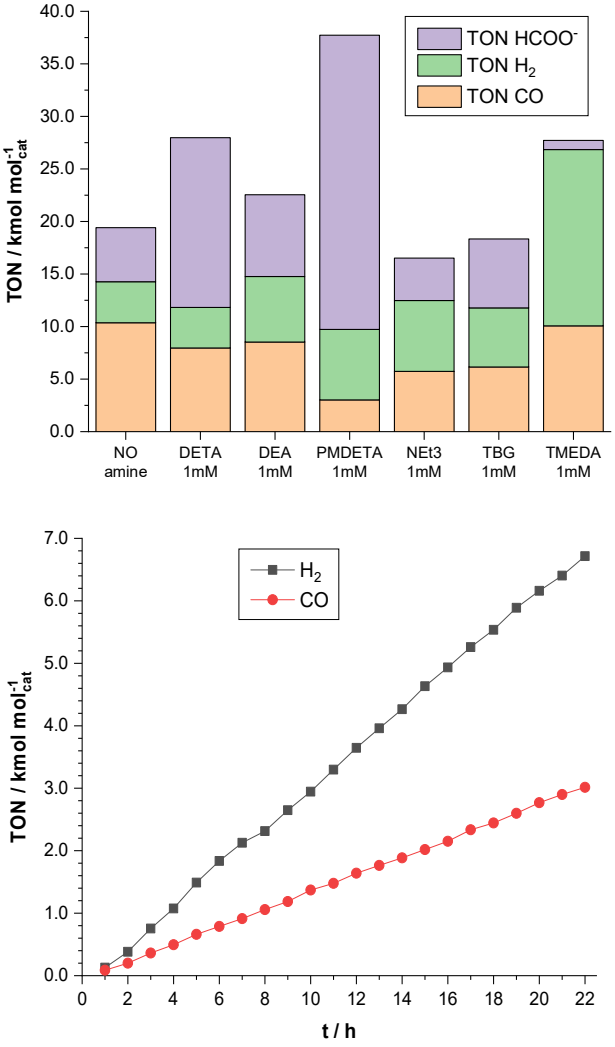

Figure 3: Overall efficiencies after 22 hours for the amines represented in Figure 2 (up). TON time profile for **Mn/CC** with PMDETA under continuous flow of CO_2 (bottom).

Within the series tested, **DETA** induced a significant increase in CO_2 selectivity to formate, reaching high FE_{HCOO-} of 51%, while **DEA** had no significant effect on the catalyst's activity or selectivity (FE_{HCOO-} = 25%). The most striking results were obtained by the addition of **PMDETA**, which strongly shifted the selectivity of **Mn/CC** towards formate, with a remarkable FE_{HCOO-} of 66%. Noteworthy, while FE_{H2} of **DETA**, **DEA** and **PMDETA** are similar (12, 21 and 11%, respectively), FE_{CO} values of **PMDETA** is significantly lower (5%). The main difference between the three amines is that **PMDETA** presents three tertiary amine functionalities, which orients CO_2 capture exclusively toward carbonation (eq.2, Scheme 1). For this reason, three other tertiary amines or guanidine were tested at the very same concentration: **TEA**, **TMEDA** and **TBG**. These species respectively present one, two and three tertiary amine functionalities, which are conjugated into a guanidine pattern in the latter. Surprisingly, these additives did not induce an increase in the production of formate compared to the amine-free reference system. In contrary, **TMEDA** displayed an

Energies	Name	Structure
0.00	**(Mn-H⁻···CO_2)** **(HMn^- + CO_2)**	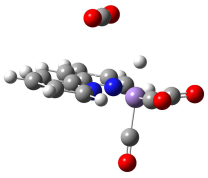
11.0	**$(Mn···H^-···CO_2)^{TS}$** TS: -448 cm^{-1}	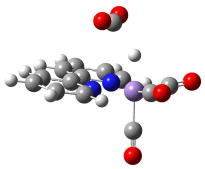
-57.4	Intermediate **($Mn···H\text{-}CO_2^-$)**	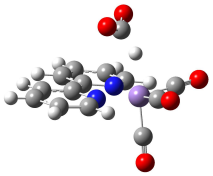
-54.5	**$(Mn\ \ H\text{-}CO_2^-)^{TS}$** TS: -30 cm^{-1}	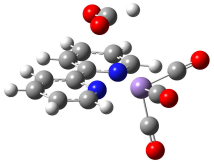
-78.4	Formate complex **($Mn···OCHO^-$)**	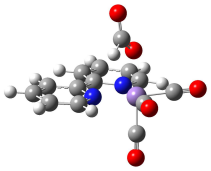
	reactant	product
	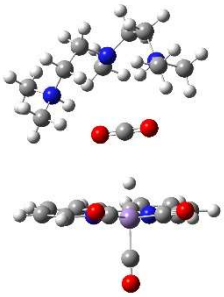	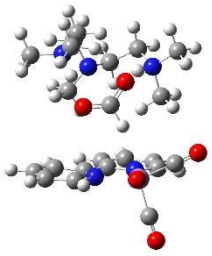

Table 3: Computed structures and relative energies (in KJ/mol) for the mechanism leading to formate. All the species are radical anions. Bottom row depicts reactant and product of the barrierless reaction **2c-PMDETA** + CO_2 + HMn^- → **2c-PMDETA** + $[CO_2HMn]^-$.

unexpected detrimental effect on formate production, yielding TON_{CO} values similar to those obtained in the absence of amine, and a noticeable increase in FE_{H2} and TON_{H2}. **TEA**, **TMEDA** and **TBG** reached TON_{HCOO-} values of 4040, 873 and 6563, and TON_{CO} of 5735, 10073 and 6159, respectively. From this set, it appears that **PMDETA** was the most efficient catalytic additive, favoring the reduction of CO_2 into formate in methanolic solutions with high TON and FE.

Daasbjerg and coworkers[46] demonstrated that, in homogeneous conditions, the active catalytic species $[Mn(bpy)(CO)_3]^-$ (**Mn^-**) reacts in acetonitrile with the starting neutral complex $[Mn(bpy)(CO)_3Br]$ (**Mn**) producing directly the neutral dimer, a key intermediate in the electrochemical reduction of the Mn bipyridyl complexes. We hypothesized that in the present case, MeOH can transform $[Mn(bpy)(CO)_3]^-$ into the corresponding hydride $HMn(bpy)(CO)_3$, namely **HMn**, since the Mn catalyst is locked on the **CC** surface and it is unlikely to react with another Mn unit.

Selected DFT calculations, performed to explain the main trends and elucidate the underpinning mechanisms, clearly indicate that the proton of MeOH points towards the metal center of the pentacoordinated $[Mn(bpy)(CO)_3]^-$ complex, and that the chemical reaction $[Mn(bpy)(CO)_3]^-$ + CO_2 + MeOH → $[HMn(bpy)(CO)_3]$ + $MeCO_3^-$ displays a favorable ΔG = –55.0 KJ/mol (see supporting section 8).

NMR analyses performed on amine samples at different concentration in CD_3OD but with a fixed 50 mM D_2O provided some clues about the species that may be present in the cathodic compartment and on their relative abundance (supporting section 7). On average, amines can be loaded with around 0.3 – 0.4 eq of CO_2 per nitrogen site at 500 mM. This loading does not vary substantially upon dilution with CO_2-saturated CD_3OD containing 50 mM D_2O, as attested by measurement of the protonation state (from ^1H chemical shift and potentiometry) and by the absence of stripping. For amines bearing primary and secondary nucleophilic nitrogen binding sites such as **DEA** and **DETA**, dilution from 500 to 5 mM globally switches the CO_2 fixation pathway, from carbamation to carbonation. At high alkalinity/amine concentration, methyl carbonate $MeCO_3^-$ is observed as a carbonation side product. For **PMDETA**, a 1.05:1.00 HCO_3^-: amine molar ratio is obtained (see SI), which validates the formation of catalytic amounts of biprotonated **PMDETA**, named **2c-PMDETA** (see Figure 4 and discussion below). At the working potential of –1.35 V, the hydride complex **HMn** is reduced to its corresponding electron-rich radical anion **HMn^-**, which is the real catalyst for CO_2 to formate conversion. DFT calculations indicate that the irreversible reduction potential of **HMn** is less negative by ~65 mV than that of the corresponding Mn dimer.

By using **Mn^-** as model, DFT calculation performed at high level def2-TZVP basis set allowed us to elucidate the two mechanisms depicted in Scheme 2, in MeOH as solvent. The path leading to CO passes through the coordination of the weak electrophile CO_2 to the strong nucleophile **Mn^-** (described in the SI), whereas the formate production in MeOH proceed via the hydride **HMn** and its reduced form **HMn^-**. Table 3 summarizes the relevant intermediates and Transition States found for this system. The first step consists into the weak coordination of CO_2 to the **HMn^-** radical anion. The adduct (**$Mn\text{-}H^-···CO_2$**) produces the intermediate (**$Mn···H\text{-}CO_2^-$**), which is 57.4 KJ/mol more stable than the (**$Mn\text{-}H^-···CO_2$**) precursor, via the transition state **$(Mn···H^-···CO_2)^{TS}$**. The energy barrier is only 11.0 KJ/mol. Thus, in MeOH, formate coordinates to the metal preferentially by its hydrogen rather than its oxygen atom, at least as a first step. Subsequently, the complex rearranges, passing through another transition state in which the formate rotates: the energy of $(Mn···H\text{-}CO_2^-)^{TS}$ is only 2.9 KJ/mol higher than the

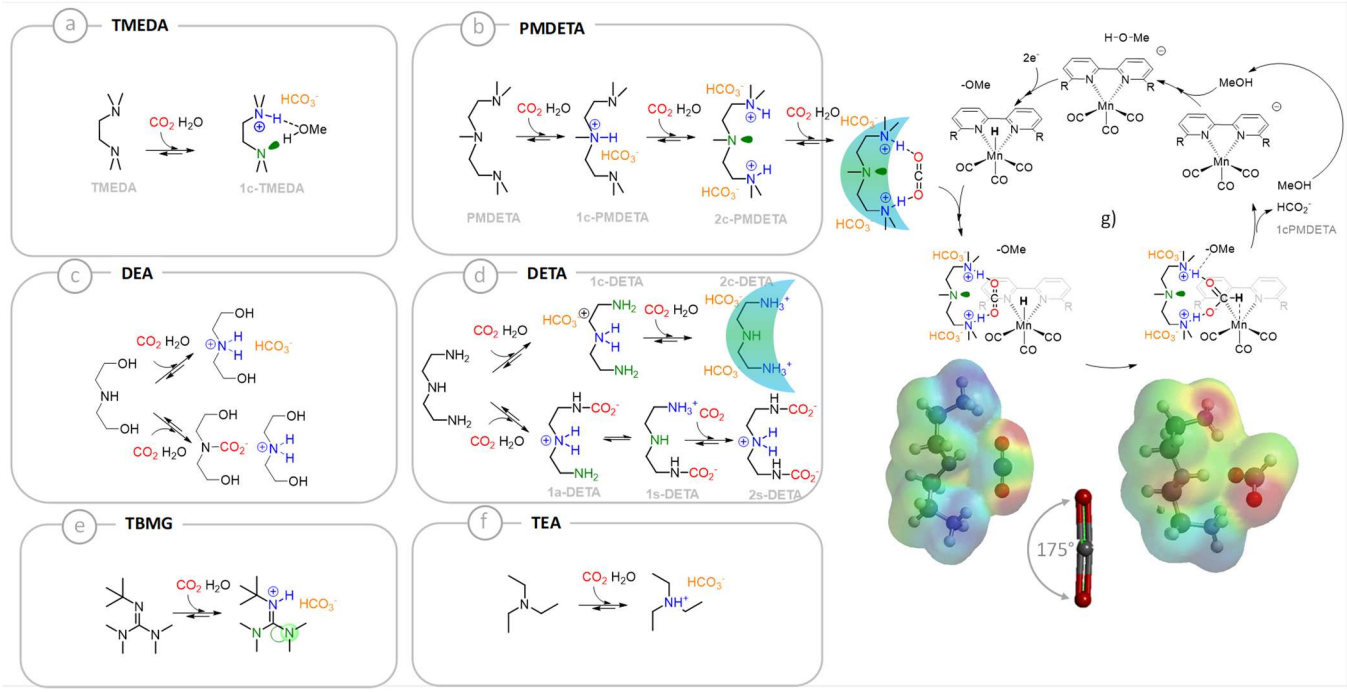

Figure 4: Interpretation of the selectivity observed from the set of amines used in this work. Frames a)-f) display the members of the carbamate and carbonate libraries generated upon CO_2 capture by each absorbent at 1 mM in methanolic solutions containing 50 mM of water. The green-cyan arch symbolizes the quadrupolar profile of bisammonium **2c-PMDETA**, d) which displays electrostatic complementarity for CO_2 and activates its reaction with the hydride generated from methanol on the supported Mn catalysts.

intermediate (**Mn···H-CO_2^-**), (54.5 KJ/mol lower in energy with respect the starting (**Mn-H^-···CO_2**) adduct). The final formate complex (**Mn···$OCHO^-$**) is more stable than the starting species by 78.4 KJ/mol. Subsequent release of formate anion and electron transfer restores the starting radical anion catalyst **Mn^-** . The mechanism leading to the coordination of CO_2 to **Mn^-** displays a similar energy barrier (10.0 KJ/mol, see supporting section 8).

As mentioned earlier, adducts generated from diluted amine-CO_2 solutions (Figure 4 a-f) should take part in this catalytic scenario, by either activating some reactive species (such as dissolved CO_2) and/or by stabilizing key transition states. With the exception of **TMEDA**, all amines display a similar TON_{H2}. This strongly suggests that the main source of protons in solution is MeOH rather than the ammonium moieties paired with carbamates or carbonates.[36, 37]

TMEDA stands as an extreme case in the series, markedly favoring H_2 over formate. The conversion of this α,β-diamine into a bisammonium dication upon double carbonation is strongly disfavored, therefore its main adduct with CO_2 combines a basic nitrogen moiety and an ammonium group (species **1c-TMEDA**, Figure 4a). This Lewis acid-base pair (or dipole) can activate the reactivity of the MeOH dipolar species toward **HMn**, thereby leading to an increased H_2 production. **PMDETA**, which formally results from the chain elongation of **TMEDA**, should act similarly. Yet, dicarbonation does occurs in substantial amount on this species, yielding an α,ω-bisammonium bearing a central neutral nitrogen (Figure 4b, **2c-PMDETA** and supporting section 7). This quadrupolar species perfectly meets the requirements to activate a complementary quadrupolar species, such as CO_2 (Figure 4b and 4g). Preliminary calculations at the AM1 level (Figure 4g, bottom) confirm this electrostatic complementarity and affinity (with the starting material, dissolved CO_2, and the product, the formate anion). It also highlights the activating role of **PMDETA**, as CO_2 binding is accompanied by its bending by 5°, which pre-activates this substrate toward hydride addition (figure 4g, bottom).

Additional DFT calculations confirm this interpretation. The divalent ammonium-bicarbonate salt **2c-PMDETA** does not only bind quite strongly to CO_2 (computed ΔG=-9.7 KJ/mol), but the reaction with the reduced Mn hydride radical anion **HMn^-** proceeds barrierless toward the production of formate, which is coordinated to Mn metal via the H atom (see last row in Table 3). The catalytic cycle then proceeds as previously described and illustrated in Table 3. Thus, the limiting step of the whole catalytic cycle is apparently no longer CO_2 activation, but the competing coordination of CO_2, bicarbonate, formate and water to **2c-PMDETA**. Indeed, DFT calculations suggest high formation constants between **2c-PMDETA** and bicarbonate (–126.9 KJ/mol) and formate (–129.8 KJ/mol).

The model described in this paragraph, based on the ability of absorbents to generate dipolar or quadrupolar CO_2 capture adducts in significant amounts, which should respectively activate complementary dipoles or quadrupoles such as methanol or CO_2 and enhance the production of H_2 or formate, remains valid on the rest of the series. **DETA** stands in between the two extreme cases of **PMDETA** and **TMEDA** and moderately enhances the selectivity toward formate production. We recently reported that **DETA**-CO_2 is a compositionally complex system in methanol[6] which is herein even further complexified by the presence of water (Figure 4c). While some methanol

activating dipolar patterns can be found on some members of the **DETA**-based library of carbamates and carbonates (such as species **1c-DETA**, **1a-DETA** and **1s-DETA,** Figure 4d), the presence of appended charges or polar moieties seems to prevent any enhancement of H_2 production. The bisammonium biscarbonate homologue of the **2c-PMDETA** adduct, noted **2c-DETA** is present in this complex system, but its relatively lower concentration and higher hydrophilicity (which decreases the availability of the ammonium moieties for lone pair binding) moderates the enhancing effect toward formate production. The other amines of the series behave as negative controls (Figure 4c, 4e and 4f): triethylammonium only displays a single acidic site while the free doublets on **TBG** are orthogonal to the lone pair of the only free nitrogen site. **DEA** bears two alcohol end groups, which may act as moderate H-bond donating sites, but in its loaded form, it misses the central nucleophilic nitrogen, to properly play the co-factor role imputed to **2c-PMDETA** quadrupole.

Conclusions

To the best of our knowledge, this study proposes the first example of a covalently bound organometallic complex employed for CO_2 reduction in the presence of amines in methanolic medium. Compared to previous integrated CO_2 capture and electroreduction processes, the current system opens the possibility of scaling up the entire carbon capture and recycling process employing a cost-effective Mn-based electrocatalyst. The abrupt increase of FE_{HCOO-} and TON_{HCOO-} values obtained by employing **PMDETA** as additive represents a breakthrough in CO_2 catalytic activation. The experimental data is supported by DFT calculations, which indicate a barrierless conversion of CO_2 to formate in our operating conditions. A lock-and-key mechanism effectively explains the role of CO_2-loaded amines in the activation of either dipolar (methanol) or quadrupolar (CO_2) substrates towards the reaction with the Mn catalyst.

We believe that this evidence paves the way towards further improvements in the CO_2-to-formate conversion with electrochemical and chemical approaches, providing that higher CO_2 concentrations and facilitated release of formate from **2c-PMDETA** can be reached.

Author Contributions

A.T. and L.R. synthesized and characterized Mn/CC. F.M.S, A.T. and L.R. performed electrochemical, CPE experiments. A.T. and L.R. processed the μGC data. F.M.S. studied the carbonation equilibrium of amine in methanol and performed NMR experiments. R.G, C.N. and J.L. designed the experiments and wrote the paper. All the authors contributed to the improvement of the manuscript.

Conflicts of interest

There are no conflicts to declare.

Acknowledgements

This work was supported by the LABEX iMUST (ANR-10-LABX-0064) of Université de Lyon, within the program "Investissements d'Avenir" operated by the French National Research Agency (ANR).

Notes and references

1. F. Marocco Stuardi, F. Macpherson and J. Leclaire, *Curr. Opin. Green Sust. Chem.*, 2019, **16**, 71-76.
2. Mission Innovation CCUS Report: Accelerating breakthrough innovation in carbon capture, utilization, and storage. 2018. https://www.energy.gov/fe/downloads/accelerating-breakthrough-innovation-carbon-capture-utilization-and-storage.
3. *USA Pat.,* US1783901A, 1930.
4. G. T. Rochelle, *Science*, 2009, **325**, 1652-1654.
5. T. M. McDonald, J. A. Mason, X. Kong, E. D. Bloch, D. Gygi, A. Dani, V. Crocellà, F. Giordanino, S. O. Odoh, W. S. Drisdell, B. Vlaisavljevich, A. L. Dzubak, R. Poloni, S. K. Schnell, N. Planas, K. Lee, T. Pascal, L. F. Wan, D. Prendergast, J. B. Neaton, B. Smit, J. B. Kortright, L. Gagliardi, S. Bordiga, J. A. Reimer and J. R. Long, *Nature*, 2015, **519**, 303-308.
6. J. Septavaux, C. Tosi, P. Jame, C. Nervi, R. Gobetto and J. Leclaire, *Nature Chemistry*, 2020, **12**, 202-212.
7. G. A. Olah, G. K. S. Prakash and A. Goeppert, *J. Am. Chem. Soc.*, 2011, **133**, 12881-12898.
8. N. M. Rezayee, C. A. Huff and M. S. Sanford, *J. Am. Chem. Soc.*, 2015, **137**, 1028-1031.
9. M. Liu, A. Hohenshil and G. Gadikota, *Energy & Fuels*, 2021, **35**, 8051-8068.
10. J. Kothandaraman, A. Goeppert, M. Czaun, G. A. Olah and G. K. S. Prakash, *J. Am. Chem. Soc.*, 2016, **138**.
11. A. Perazio, G. Lowe, R. Gobetto, J. Bonin and M. Robert, *Coord. Chem. Rev.*, 2021, **443**, 214018.
12. Y. Yamazaki, H. Takeda and O. Ishitani, *J. Photochem. Photobiol. C: Photochem. Rev.*, 2015, **25**.
13. E. Boutin, L. Merakeb, B. Ma, B. Boudy, M. Wang, J. Bonin, E. Anxolabéhère-Mallart and M. Robert, *Chem. Soc. Rev.*, 2020, **49**, 5772-5809.
14. C. Costentin, M. Robert and J.-M. Saveant, *Chem. Soc. Rev.*, 2013, **42**, 2423-2436.
15. N. Armaroli and V. Balzani, *Chem. Eur. J.*, 2016, **22**, 32-57.
16. B. Hu, C. Guild and S. L. Suib, *J. CO2 Util.*, 2013, **1**, 18-27.
17. F. Franco, C. Rettenmaier, H. S. Jeon and B. Roldan Cuenya, *Chem. Soc. Rev.*, 2020, **49**, 6884-6946.
18. L. Rotundo, R. Gobetto and C. Nervi, *Curr. Opin. Green Sust. Chem.*, 2021, **31**.
19. T. Yoshida, K. Kamato, M. Tsukamoto, T. Iida, D. Schlettwein, D. Wöhrle and M. Kaneko, *J. Electroanal. Chem.*, 1995, **385**, 209-225.
20. T. Abe, T. Yoshida, S. Tokita, F. Taguchi, H. Imaya and M. Kaneko, *J. Electroanal. Chem.*, 1996, **412**, 125-132.
21. J. Grodkowski, P. Neta, E. Fujita, A. Mahammed, L. Simkhovich and Z. Gross, *J. Phys. Chem. A*, 2002, **106**, 4772-4778.
22. J. Hawecker, J. M. Lehn and R. Ziessel, *J. Chem. Soc., Chem. Commun.*, 1984, DOI: 10.1039/C39840000328, 328-330.
23. J. M. Smieja and C. P. Kubiak, *Inorg. Chem*, 2010, **49**, 9283-9289.
24. M. Bourrez, F. Molton, S. Chardon-Noblat and A. Deronzier, *Angew. Chem. Int. Ed.*, 2011, **50**, 9903-9906.
25. D. L. DuBois, A. Miedaner and R. C. Haltiwanger, *J. Am. Chem. Soc.*, 1991, **113**, 8753-8764.
26. D. L. Dubois, *Comments Inorg. Chem.*, 1997, **19**, 307-325.

27. J. W. Raebiger, J. W. Turner, B. C. Noll, C. J. Curtis, A. Miedaner, B. Cox and D. L. DuBois, *Organometallics*, 2006, **25**, 3345-3351.
28. F. Franco, S. Fernández and J. Lloret-Fillol, *Curr. Opin. Electrochem.*, 2019, **15**, 109-117.
29. L. Rotundo, E. Azzi, A. Deagostino, C. Garino, L. Nencini, E. Priola, P. Quagliotto, R. Rocca, R. Gobetto and C. Nervi, *Front. Chem.*, 2019, **7**.
30. M. D. Sampson and C. P. Kubiak, *J. Am. Chem. Soc.*, 2016, **138**, 1386-1393.
31. L. Rotundo, C. Garino, E. Priola, D. Sassone, H. Rao, B. Ma, M. Robert, J. Fiedler, R. Gobetto and C. Nervi, *Organometallics*, 2019, **38**, 1351-1360.
32. F. Franco, C. Cometto, F. Ferrero Vallana, F. Sordello, E. Priola, C. Minero, C. Nervi and R. Gobetto, *Chem. Commun.*, 2014, **50**, 14670-14673.
33. F. Franco, C. Cometto, L. Nencini, C. Barolo, F. Sordello, C. Minero, J. Fiedler, M. Robert, R. Gobetto and C. Nervi, *Chem. Eur. J.*, 2017, **23**, 4782-4793.
34. M. Bhattacharya, S. Sebghati, R. T. Vanderlinden and C. T. Saouma, *J. Am. Chem. Soc.*, 2020, **142**, 17589-17597.
35. C. G. Margarit, N. G. Asimow, C. Costentin and D. G. Nocera, *ACS Energy Letters*, 2020, **5**, 72-78.
36. J. B. Jakobsen, M. H. Rønne, K. Daasbjerg and T. Skrydstrup, *Angew. Chem. Int. Ed.*, 2021, **60**, 9174-9179.
37. M. H. Rønne, D. Cho, M. R. Madsen, J. B. Jakobsen, S. Eom, É. Escoudé, H. C. D. Hammershøj, D. U. Nielsen, S. U. Pedersen, M.-H. Baik, T. Skrydstrup and K. Daasbjerg, *J. Am. Chem. Soc.*, 2020, **142**, 4265-4275.
38. N. Morlanes, K. Takanabe and V. Rodionov, *ACS Catal.*, 2016, **6**, 3092-3095.
39. B. Reuillard, K. H. Ly, T. E. Rosser, M. F. Kuehnel, I. Zebger and E. Reisner, *J. Am. Chem. Soc.*, 2017, **139**, 14425-14435.
40. L. Rotundo, J. Filippi, R. Gobetto, H. A. Miller, R. Rocca, C. Nervi and F. Vizza, *Chem. Commun.*, 2019, **55**, 775-777.
41. J. Filippi, L. Rotundo, R. Gobetto, H. A. Miller, C. Nervi, A. Lavacchi and F. Vizza, *Chem. Eng. J.*, 2021, **416**, 129050.
42. E. Antolini, *Appl. Catal. B*, 2009, **88**, 1-24.
43. N. McCann, M. Maeder and H. Hasse, *Energy Procedia*, 2011, **4**, 1542-1549.
44. M. Décultot, A. Ledoux, M.-C. Fournier-Salaün and L. Estel, *J. Chem. Thermodyn.*, 2019, **138**, 67-77.
45. C. Riplinger, M. D. Sampson, A. M. Ritzmann, C. P. Kubiak and E. A. Carter, *J. Am. Chem. Soc.*, 2014, **136**, 16285-16298.
46. M. H. Rønne, M. R. Madsen, T. Skrydstrup, S. U. Pedersen and K. Daasbjerg, *ChemElectroChem*, 2021, **8**, 2108-2114.